International Conference on Space Optics—ICSO 2022

Dubrovnik, Croatia

3–7 October 2022

Edited by Kyriaki Minoglou, Nikos Karafolas, and Bruno Cugny,

10 Gbps free space optical communication link using Multi-Plane Light Conversion turbulence mitigation

10 Gbps free space optical communication link using Multi-Plane Light Conversion turbulence mitigation

Antonin Billaud[a], Adeline Orieux[a], Fausto Gomez[a], Thibault Michel[a], Stephane Bernard[a], David Allioux[a], Olivier Pinel[a]

[a]Cailabs, 1 rue Nicolas Joseph Cugnot, 35000 Rennes, FRANCE

ABSTRACT

Satellite constellations, whether for high-speed Internet access or for Earth observation using high-resolution imagery, are leading to a sharp increase in the volume of data to be brought back to Earth. To meet the needs of these very high-speed communication links, from 10 Gbps to 1 Tbps, optical technologies are becoming essential. Radio frequency technologies currently in use can no longer cope with such data rates without threatening the allocation of frequencies on Earth (5G-6G) or in space. However, to work at high debit rates, broadband optical communication systems require small detectors, high performance amplifiers or coherent modulation schemes needing high efficiency coupling into SMFs, which is subject to atmospheric turbulence. Using Cailabs' core technology, Multi-Plane Light Conversion (MPLC), followed by a photonic integrated chip optical recombiner, we have developed and qualified a unique component for turbulence compensation.

This architecture provides high-speed turbulence mitigation at several kHz with the advantage of a single SMF output. In this paper, we investigate the fading improvement provided by this system over direct single mode fiber coupling under various environmental conditions and technical implementations. This system is tested on a km-long test link at Cailabs at up to 10 Gbps under appropriate environmental conditions and at higher debit rates on a turbulence emulation bench. Several configurations are evaluated, including several levels of turbulence. Meanwhile, Cailabs is building its first optical ground station for the LEO-ground optical link. We will present the first experimental results obtained and the roadmap for satellite-ground communication.

Keywords: Laser Communication, Multi-Plane Light Conversion, Atmospheric turbulence, Free-Space Optical Communication.

1. INTRODUCTION

Increased demand for hight-thoughput data transfer is driven by the rapid deployment of telecommunication and high-resolution earth observation satellite constellations. Free-space optical communication (FSOC) providing high debit based on pre-existing telecom components is seen as a relevant solution for these links beyond 10 Gbps. However, such throughputs depend on small size detectors and other fiberized components such as EDFAs and coherent detection schemes which are only compatible with a single mode fiber output. Atmospheric turbulence impairing free space to single mode fiber coupling, turbulence mitigation schemes are required for >10 Gbps throughput. To ensure reliability and high speed for FSOC links, one needs good optical beam quality at the receiver side for multiple reasons such as compatibility with high speed detectors (>10Gbaud) or integration with off-the-shelf telecom systems.

The most straightforward way to increase throughput is by increasing debit rate in an OOK modulation format (ie. increasing the baud rate) which requires the use of smaller detectors the higher the debit rate. However, atmospheric turbulences induce uncontrolled beam perturbation, transforming a single mode input beam with an M^2 close to one into a randomly varying shape. At the focal plan of the receiving telescope from a FSO link such a distorted beam can have a typical size much bigger than the expected Airy pattern diameter, by up to one or two orders of magnitudes, with a rapidly varying shape and general movement of the beam's center of mass. Allowing active and real-time correction of the distorted beam to bring its Airy pattern close to diffraction limited is therefore imperative for high-debit capabilities.

Further debit rate increase can also be achieved through the use of more complex modulation schemes such as coherent detection. This kind of modulation is based on encoding information on phase (phase modulation instead of amplitude modulation) and thus interferometry is compulsory to retrieve the data. However, proper interferometry is only possible when the two interfering beams have similar shape and modal content. Thus, compatibility with SMF technology is compulsory.

Moreover, compensating a distorted beam so that it becomes compatible with an single mode fiber with low injection losses allows for many benefits. This permits the use of smaller detectors - hence higher debit rate (in pulses / sec) -, more complex modulation schemes -hence higher debit rate (in bits / pulse) – and compatibility with standard fiberized components such as EDFA - hence better SNR.

2. A NOVEL APPROACH TO TURBULENCE MITIGATION

Classical aberrations of optical beams are often described using the Zernike polynomials which allow decomposition of the phase profile [1]. More generally, a complex field can be decomposed on any arbitrary spatial mode base [2]; thus a turbulent beam can be described as a linear combination of modes of the selected mode basis with the complex factors of each mode varying over time with atmospheric turbulences fluctuation as shown on Figure 1.

Figure 1. Example of modal decomposition of a turbulent beam

Using a Multi-Plane Light Converter (MPLC) [3] to act as a spatial demultiplexer is therefore highly relevant passive solution for turbulence mitigation as it allows conversion of one mode base into another, thus offering a way towards improvement of coupling efficiency of a perturbated beam into SMFs. Indeed, a perturbated beam is a combination of modes, e.g. HG modes [4], which can be transformed individually in spatially separated TEM00 modes as shown on Figure 2.
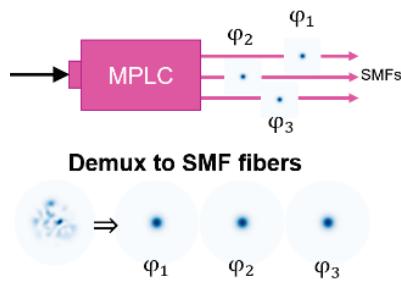

Figure 2. Demultiplexing of high orders modes into multiple TEM00 implemented by the MPLC

After the perturbated beam is coupled in a series of SMFs, these can be either sent on individual high-speed detectors [5] and numerically summed [6-7] or be optically combined through coherent combining to keep compatibility with SMF of the input signal [8-10]. The first solution offers ease of implementation but shows some limitations such as complexity of the required high-speed electronics depending on the throughput rate, high pricing due to a potentially high numbers of detectors and low compatibility with coherent detection schemes. The second solution offers a more future-proof approach but requires the use of an active optical coherent combining scheme to merge the SMFs signals.

3. SYSTEM DESCRIPTION

Figure 3 shows a turbulence mitigation scheme based on the second approach previously described and made of two modules: a MPLC which passively demultiplexes the turbulent beam into a set of gaussian beams and an active combining unit which merges all the gaussian beams into a unique one that can be injected into a PM-SMF fiber. Demonstration of the use of an MPLC for demultiplexing of a turbulent beam was previously demonstrated [5-7,11]. By collecting light from different spatial modes, collection efficiency of a turbulent beam is improved whilst is decreased in amplitude and frequency. Decreasing fading is quite important as these fast and high fluctuations of collected power create short breaks of the telecom light, forbidding the use of high debit rates.
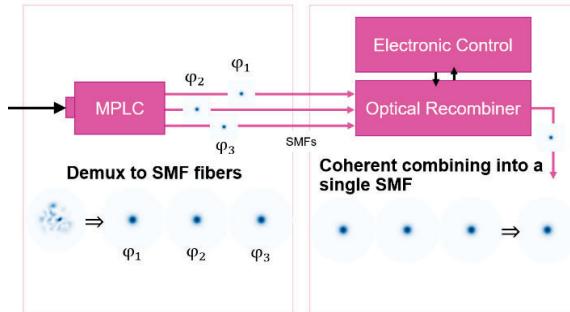
Figure 3. Turbulence mitigation scheme based on a MPLC and a coherent combining unit

3.1 MPLC

MPLC is a technique that allows performing any unitary spatial transform [3]. Thanks to a succession of transverse phase profiles, each separated by a free-space propagation serving as a Fourier transform, it enables the conversion of any set of N orthogonal spatial input modes into any arbitrary set of N orthogonal output modes. MPLC principle is shown schematically in Figure 4.
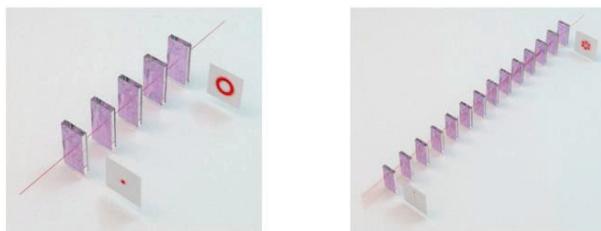

Figure 9. Multi-Plane Light Conversion principle, single-mode (left) and multi-mode (right)

In particular, MPLC enables mode selective spatial multiplexing and demultiplexing, i.e. conversion of N spatially separate input Gaussian beams into N orthogonal modes, typically Hermite-Gaussian or Laguerre which can be overlapping [12]. Experimentally, MPLC is implemented using a multi-pass cavity, in which the successive phase profiles are all manufactured on a single reflective phase plate. Figure5 (left) shows a picture of a real MPLC. Cavity is formed by a mirror and the reflective phase plate, noticeable with its gold coating on Figure 5. A MPLC used in reverse direction implements the demultiplexing operation. This system can be made embeddable and compact as shown on Figure 5 (right) with a footprint of few square centimeters.
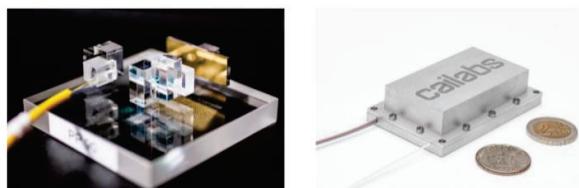

Figure 5. Photo of an MPLC (Left) and footprint of a compact MPLC (Right)

3.2 Optical Combiner

The optical combiner is an active system designed to coherently combine all the polarization maintaining single-mode fibers (PM-SMF) exiting the MPLC. As the input signals of the combiner are temporally fluctuating in phase and amplitude due to turbulence variations, an active system must provide real-time adjustment of phase and power distribution in order to reach high efficiency combining. This is achieved through Mach-Zehnder interferometers which are used for two-by-two combining. Such interferometer possesses a phase shifter before the interferometer and one inside as shown on Figure 6.
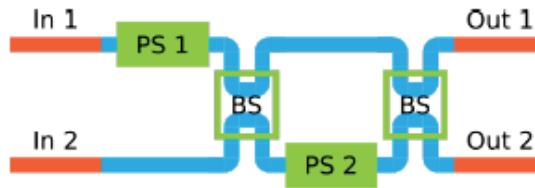

Figure 6. Two-by-two channels recombining principle using a Mach-Zehnder interferometer

The first phase shifter (PS) allows adjustment of energy distribution between the two waveguides after the first beam splitter (BS), distributing it evenly between top and bottom arms. Second phase shifter controls phase difference between the two arms, ensuring phase matching when reaching the second BS. If phase matching is well achieved all the light comes out through one output. If they are in phase opposition, light will come out through the other output. Thus this system allows us to redirect all the optical power into one output for any power and phase distribution between the two inputs. Such a system for active combining of two fluctuating inputs was previously demonstrated with fiberized electro-optic phase shifters [13].

This design was implemented here on a photonic integrated chip (PIC) manufactured on SOI platform. This required the use of PM-SMFs as only one polarization was guided in the chip's waveguides. The full system was designed to allow coherent combining of up to 8 channels and is shown on Figure 7.
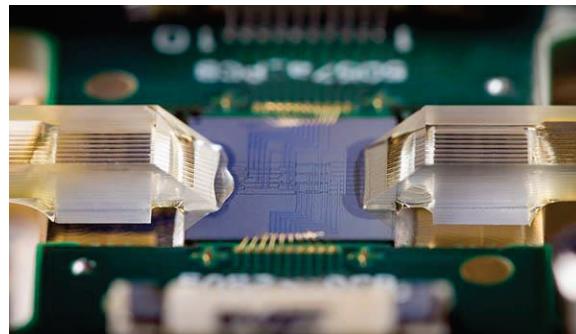

Figure 7. Close view of a photonic integrated chip (PIC) with vertical coupling through grating couplers

4.   KILOMETER-LONG EXPERIMENTAL SETUP

4.1 Emission and reception design

Turbulence mitigation system was tested on a real experiment link. Real conditions are both more representative and more complicated to set up than turbulence bench as many unpredictable problem may appear. These issues can be related to beam divergence, power in the receiver aperture, fine alignment between Tx & Rx, active alignment correction and so on. To remove some of these problems we opted for a symmetrical architecture based on two 20 cm telescopes; this offers the advantage of low beam divergence, standard tracking control availability from astronomy telescope mounts and ease of interfacing via cage mount systems.

Figure 8 shows the emission side of this optical link. It comprises a transmitter, which can be switched between a CW laser and a telecom laser, a 2-lens telescope for adapting laser mode size to the Kepler telescope numerical aperture and a beam splitter. The beam splitter allows us to have a monitoring arm used for checking alignment via an infrared camera.
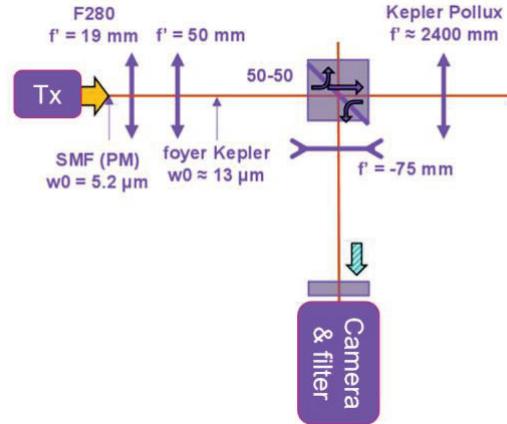

Figure 8. Schematic of the emission side of a 200 m FSO link

Figure 9 shows the receiver side with a more complex setup. It first comprises a beam splitter to allow monitoring of the turbulent beam via an infrared camera, which can be used for a posteriori calculation of the Fried parameter. A fast-steering mirror (FSM) is placed on the main optical path for tip-tilt correction, followed by a second 10/90 beam splitter where the 10 percent channel contains a quadrant photodiode used in the feedback loop of the FSM. The main optical path finally contains a 50/50 beam splitter after which the light is sent onto two arms, one where light is injected into a SMF and another where it is injected into an FMF which serves as input to our MPLC.
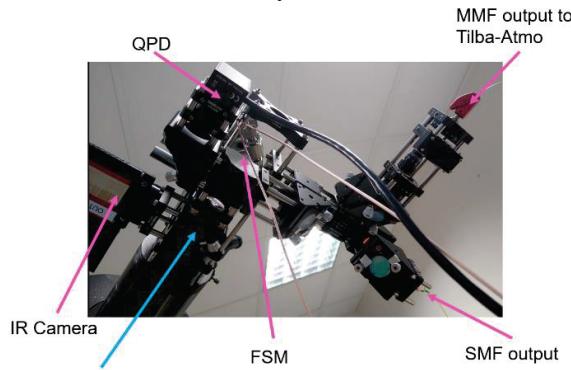

Figure 9. Receiver side of the 200 m FSO link

4.2 Kilometer-long link localization

Once the two units were ready, one for emitting and the other for receiving, we implemented a 1-km link between two buildings in the city center of Rennes, France. The buildings identified where chosen to be more than 4 stories high to ensure visibility between the two sites. Figure 10 shows the view from the emitter's end with the receiver position circled in blue while Figure 11 shows the view from the receiver's end with the emitter position circled in red. The distance between both telescope was estimated at 1.1 km.

Figure 10. Reception site seen from the emission site

Figure 11. Reception site seen from the emission site

4.3 Alignment procedure

Alignment of the two systems (receiver & emitter) is of utmost importance to ensure high optical transmission of the telecom link. The telescopes used here have a 20 cm aperture with a focal of 2.4 m which means a numerical aperture of 0.042.

The emitted beam is quite large and can be assimilated to a gaussian with a waist of around 60 mm and an associated Rayleigh range of around 7 km, ie. the beam at the receiver side would still have a diameter at three ω_0 of around 20 cm (atmospheric turbulence not taken into account). Any angular misalignment at the emission leading to a lateral shift of more than 20 cm after 1 km would forbid us from closing the link. This corresponds to a value of 200 µrad (41 arcsec). Moreover, the small numerical aperture of the receiver means that even if light reaches it, if both telescopes axes are not concentric, light will not reach the focal plane of the receiver.

To ensure both telescopes are well aligned with each other we start by aligning the finderscope (also called finder) of each subsystem such that both the telescope axis and its associated finder are colinear. The easiest method is to target something far away (like a tower or a crane) and ensure both ocular and finder are centered on this object as shown in Figure 12.

Figure 12. Finder alignment on a faraway structure

Once this is done, we can target the receiver with the emitter and inversely to ensure both systems are concentric, as both have small numerical aperture this is quite crucial.

This is quite difficult as any slight misalignment between finder and telescope will lead to pointing errors. This is particularly the case here as the emitted beam is well collimated and illuminates an area which is roughly the size of the receiver's diameter – contrary to what you could obtain on a LEO sat to ground link where the illuminated area can be tens to hundreds of meters wide.

Figure 13 (left) shows pointing of the receiver from the emitter with the finder which shows good alignment. However, due to a slight off-axis alignment of the cage-mount set-up on the telescope, leading to the cage mount system not being perfectly aligned with the telescope optical axis, a small misalignment between telescope and finder occurred which is shown on Figure 13 (right) where the telescope point of impact is represented by the red target whilst the emitted laser beam point of impact is represented by the cyan cross. A misalignment of 60cm after 1.1 km was measured corresponding to an angular difference of 600 µrad (123 arcsec) forcing us to manually look for the beam at the receiver site and then compensate with the telescope used for emission.
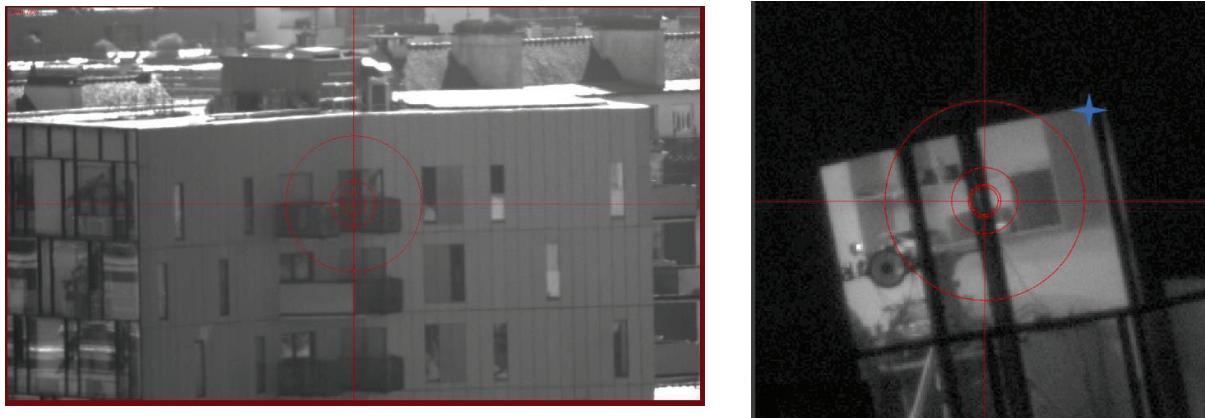

Figure 13. Telescope alignment (left) and telescope and laser misalignment at receiver's side (right)

4.4 Turbulence evaluation

We evaluated the amount of turbulence from a camera put at the receiver's end an comparing the instantaneous Point spread function (PSF) of the system compared to the one obtained in laboratory condition when no turbulence is present. To do so we aligned the two telescope (emitter & receiver) in front of each other with only 50 cm free space propagation in between and we observed the PSF as showed in Figure 14 in linear and log scale:
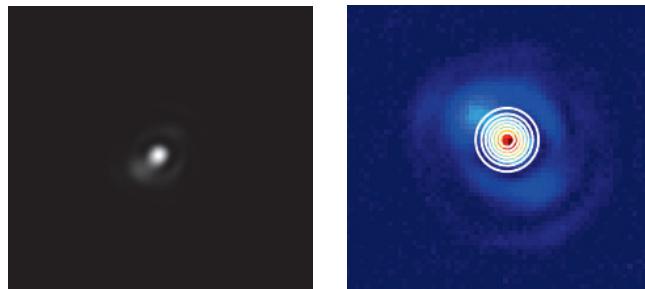

Figure 13. Receiver system PSF without turbulences in linear (left) and log (right) scale

One can observe that the PSF obtained is close to an Airy pattern but is not perfect. This is due to both telescopes having central extinctions, i.e. on the emitter side we emit a gaussian beam whose center has been removed and on the receiver side we collect a donut pattern which PSF is not an Airy pattern. Moreover, optical and optomechanical misalignments of the global system will also result in deformation of the PSF.

Here are some of the pictures obtained during our measurement campaign in April 2022 in Rennes, France. Figure 14 shows images of the turbulent beam obtained on the 20th of April at 10pm CET and Figure 15 shows the same measures on 25th of April at 2:40 pm CET. Black and white pictures show instantaneous images whilst the colored ones show long time exposure.
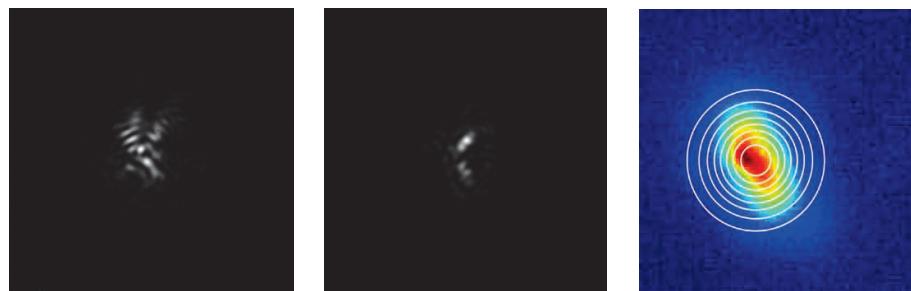

Figure 14. Instantaneous pictures of the turbulent beam (left and center) and long-time exposure (right) on the 20th of April at 10pm CET corresponding to Fig 19 results
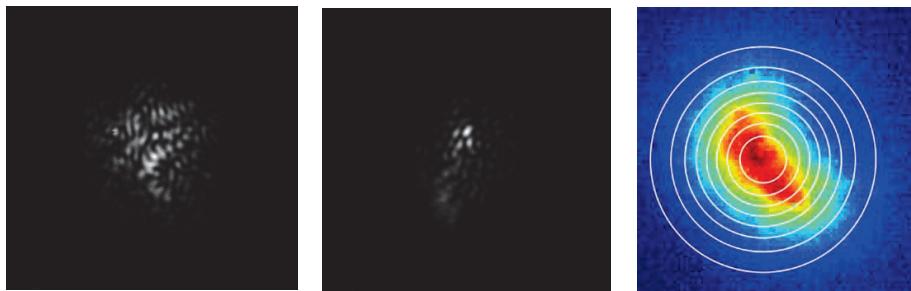

Figure 15. Instantaneous pictures of the turbulent beam (left and center) and long-time exposure (right) on the 25th of April at 2:40pm CET

4.5 Turbulence bench for 100Gbps DP-QPSK testing

The system was also tested on a turbulence bench developed at Cailabs already presented in previous work [8], which is quite similar in its design to the PICOLO turbulence bench at the ONERA [14]. Figure 16 shows a schematic of the PICOLO setup where up to three phase plates representing different layers of the atmosphere can be placed. Each phase plate has a different r_0 (Fried parameter) and a different rotation speed, which allows to emulate the desired atmospheric profile and its corresponding Greenwood frequency by simulating different layers of the atmosphere.
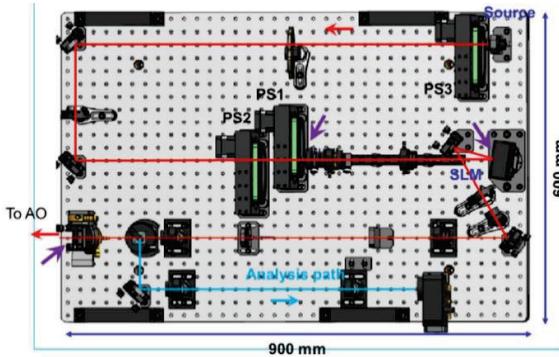

Figure 16. Schematic of the PICOLO turbulence bench at the ONERA [14]

Figure 17 (left) shows a schematic of the turbulence emulation bench developed internally which was also based on the use of rotating phase plates. The beam is collimated and then sent through the different phase plates - each having a different r_0, rotation speed and position to fit the desired Cn² profile – before being clipped in a physical pupil which defines the D/r_0 of our system. The first phase plate represents the high atmosphere and is thus a plate with a high r0 (corresponding to small amount of turbulence) and a fast rotation speed while the second phase plate represents the low atmosphere with a much smaller r0 value changing at a much slower speed. This turbulent beam can be split into two channels, the first one being injected into a SMF and the second one being injected into the MPLC aperture (which can be free-space or a FMF/MMF). Moreover, a tip-tilt compensation module was added after the injection pupil to correct for pointing instabilities, allowing better injection into the SMF and MPLC channels.

Different telescopes precede the MPLC aperture. The first one is designed to match the tip-tilt mirror aperture to ensure best pointing compensation capabilities. The second one adjusts the beam size in the focal plane where the 4-quadrant photodiode driving the tip-tilt mirror will be placed. The third and fourth ones are used to match the system's pupil with the SMF core diameter and the MPLC pupil. Figure 17 (right) show the assembled turbulence bench.
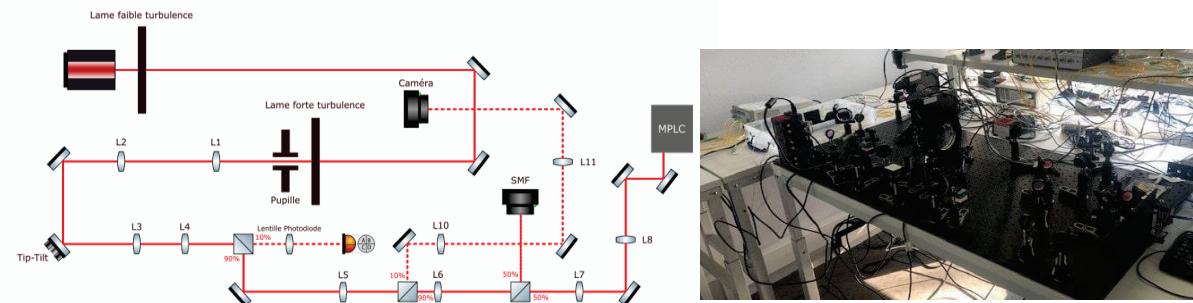

Figure 17. Cailabs' turbulence emulation bench schematic (left) and picture of it (right)

After injection in the MPLC, recombining occurs through the different elements of the TILBA-ATMO system. One of the components of the TILBA-ATMO being polarization sensitive and allowing only TE polarization to go through it, the received beam which contains two polarizations - due to the telecom modulation format used - was split into two different

sub-channels after the MPLC and each polarization was recombined independently before being merged together via a fiberized polarization beam splitter (PBS) used in reverse.

Moreover, as this combining is based on the different channels being coherent with each other, one has to ensure the different path lengths are similar to each other and below coherence length. This coherence length is here determined by the symbol rate targeted to avoid symbol mismatch and is here of 10 Gbaud/s. This corresponds to a laser pulse every 0.1 ns and equals a fiber length of roughly 2 cm. Thus, paths had to be equalized to a value much smaller than 2 cm and was achieved by the use of custom-made patchcords.

Figure 18 summarizes the setup described above in a schematic of the recombining unit where two PICs are used, one for each polarization with custom-made patchcords to deal with path-length discrepancies. Tx is performed with an Ekinops module aggregating 4x32,775 Gbaud in DP-QPSK before FEC, leading to 100 Gbps effective data rate.
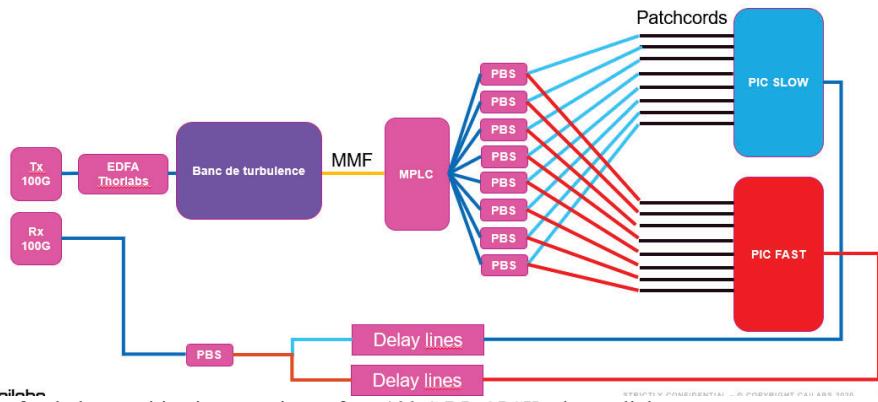

Figure 18. Schematic of turbulence mitigation experiment for a 100 G DP-QPSK telecom link

5. RESULTS

5.1 1-km long FSOC urban link

Preliminary tests were conducted on the 1.1 km link in different turbulence conditions. The first results were obtained by night where we compared the signal with an SMF receiver to a similar link with an 8-mode TILBA-ATMO system. Current version of the TILBA-ATMO system used for these tests was a laboratory version to demonstrate improvement of fading with 8 modes recombined and was not optimized in terms of losses with 10 dB optical losses, mainly due to fiber-to-chip and chip-to-fiber coupling.

This FSO turbulent link was used and characterized with a D/r0 of around 2.8 by post-processing data acquired through a camera at the receiver's end. We compared power collected in a SMF, with our unit (TILBA) and coming out of the MPLC before optical combining (Sum). An FSM was placed on the beam path and a feedback loop was running to ensure recentering of the beam. Fig.19 shows the statistical values of the results obtained where a clear improvement can be observed by using the Tilba system instead of an SMF.

The power offset shown here is arbitrary as the multiple beam paths have different optical losses. However, we can compare spreading and observe that power fluctuations can be divided by more than 3-4 dB through the Tilba system even in a case of low turbulences. This demonstrates the advantage of the solution to decrease fading on a perturbated optical link.
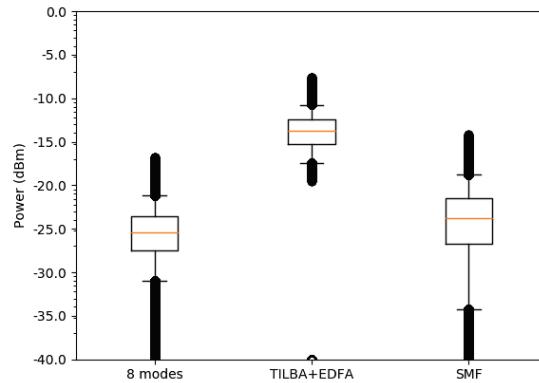
Figure 19. Statistics of collected optical power on a 1 km FSO link for an SMF, a 8-mode MPLC and a 8-mode TILBA system

5.2 100Gbps DP-QPSK coherent ling on turbulence bench

As the gain of turbulence mitigation system is greater for high data-rate, we evaluated the system at 100 Gbps in DP-QPSK coherent modulation. Test system is quit bulky and was thus first tested on Cailabs turbulence bench. The system was first tested without any tip-tilt compensation with a $D/r0$ of 1.5. As the Fried parameter size is quite close to the pupil, one can expect most of the turbulences' effect to be beam wandering with a slight amount of beam deformation.

Figure 20 shows the evolution of the output power of the TILBA-ATMO output when rotating the phase plate one full turn clockwise followed by one full turn anti-clockwise, going back to the starting position. Power fluctuations of more than 20 dB can be observed from -10 dBm down to -35 dBm at some points. The 100 Gbps telecom system used here has a detection threshold of -25 dBm and a saturation level of -10 dBm.
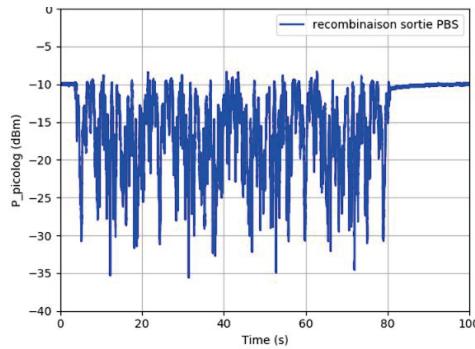

Figure 20. TILBA-ATMO output power on turbulence bench for D/r_0 of 1.5

According to the previous measurement which had a duration of 77 seconds, it was estimated that 4.4 seconds were spent below the detection threshold. We repeated this experiment for different rotation speeds of the phase plate used and the results are summarized in Table 3. Each measurement was done over 77 seconds and the number of turns was increased with rotation speed to ensure this. Therefore the amount of time where the output was below detection threshold should stay the same at 4.4 seconds or close to it as the TILBA-ATMO might be slightly less efficient for faster turbulence changes. The measured debit rate decreases heavily with rotation speed even reaching values were the link is completely non-functional at high turbulences speed.

Table 3. Evolution of debit rate with phase plate rotation speed

Speed (a.u.)	Measured debit rate	Downtime from EXFO statistics	Time below threshold
Not moving	94.7 Gb/s (100%)	NA	NA
500	69.1 Gb/s (73.0%)	20.8 s	4.420 s (5.7%)
1000	47.6 Gb/s (50.3%)	38.3 s	4.423 s (5.7%)
1500	27.1 Gb/s (28.6%)	54.9 s	4.692 s (6.1%)
2000	16.1 Gb/s (17.1%)	63.9 s	4.717 s (6.1%)
2500	3.4 Gb/s (3.6%)	74.2 s	4.810 s (6.2%)
3000	-1.4 Gb/s (-1.5%)	78.2 s	5.105 s (6.6%)

We can observe that according to the EXFO transmission tester statistics, downtime increases with rotation speed whilst time below threshold stays roughly the same as summarized on Figure 21. Thus, debit rate could be expected to remain the same for the different speed values but results show a different behavior. When increasing rotation speed we also increase the number of full rotation to keep a constant duration for each measurement which lead to an linear increase with speed in the number of events where the output power reaches a value below threshold.
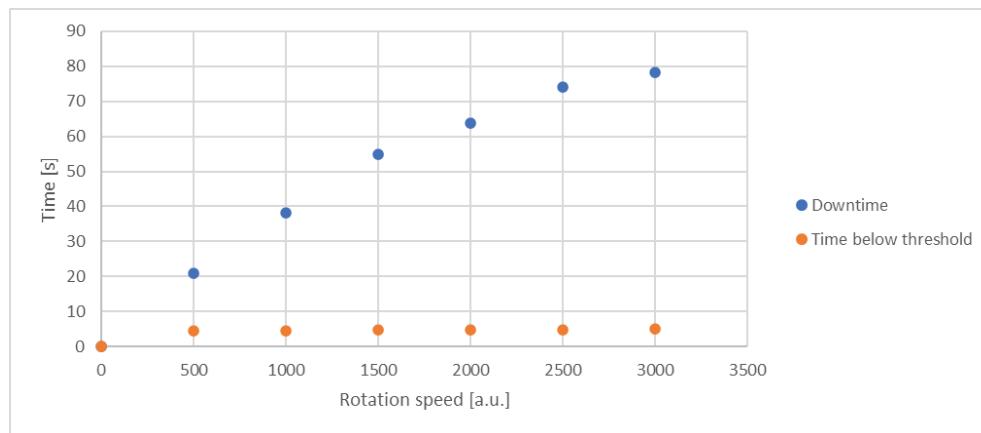

Figure 21. Evolution of link downtime and time below threshold versus phase plate rotation speed

From the previous data we deduce debit rate decreasing with turbulence speed is not due to the overall time below detection threshold but to recovering time of the transceiver after an event where the received power was below the -25 dBm threshold.

The tip-tilt module was then activated to compensate for pointing error and the previous data were acquired again. Figure 22 shows the collected power over time. The drops decreased from up to 25 dB before to less than 8 dB here.
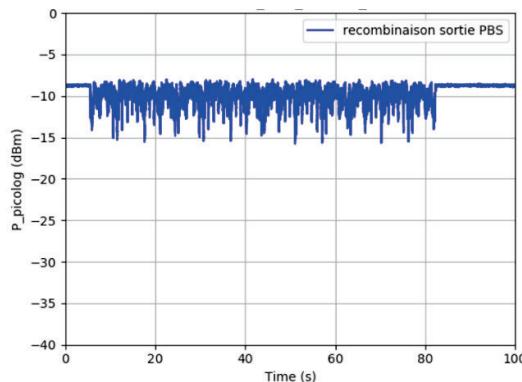

Figure 22. TILBA-ATMO output power on turbulence bench for D/r_0 of 1.5 with tip-tilt compensation

Table 4 shows the debit rates obtained for difference turbulence speeds of the phase plate. Here a decrease of debit rate of less than 10 % was observed when reaching speeds five times higher than the previous values where the link was fully down when the tip-tilt was not working.

Table 4. Evolution of debit rate with phase plate rotation speed with tip-tilt compensation

Speed (a.u.)	Measured debit rate	Downtime from EXFO statistics
3000 pps	94.64 Gb/s	0 s
6000 pps	94.65 Gb/s	0 s
9000 pps	92.0 Gb/s	5 s
12000 pps	92.2 Gb/s	4 s
15000 pps	87.1 Gb/s	12 s

6. CONCLUSION

In this article, we proposed a review of the turbulence mitigation system consisting of an MPLC spatial demultiplexer followed by a photonic integrated chip all optical recombiner. The system was tested on a turbulence bench at throughput up to 100 Gbps and on a 1 km free space optical link up. We demonstrate compatibility of the system with high data-rate and coherent modulation as well as improved fading mitigation compared to SMF coupling.

7. REFERENCES

[1] Noll, R J "Zernike polynomials and atmospheric turbulence". J. Opt. Soc. Am. 66, 207–211 (1976).
[2] Huang, B et al., "Turbulence-Resistant Free-Space Optical Communication Using Few-Mode Preamplified Receivers". 2017 European Conference on Optical Communication (ECOC) 1–3 (2017)
[3] Morizur, J-F et al., "Programmable unitary spatial mode manipulation". J. Opt. Soc. Am. A 27, 2524–2531 (2010).
[4] Cox, M A et al., "The Resilience of Hermite- and Laguerre-Gaussian Modes in Turbulence". Journal of LightwaveTechnology 37, 3911–3917 (2019).
[5] R. Mata Calvo et al., "Alternative passive fiber coupling system based on multi-plane light conversion for satellite-to-ground communications", Proc. SPIE 11272, Free-Space Laser Communications XXXII, 112720Q (9 March 2020)

[6] M. Arikawa, Y. Ono and T. Ito, "Evaluation of Blind Diversity Combining of Severely Faded Signals for High-Speed Free-Space Optical Communication under Atmospheric Turbulence," 2017 European Conference on Optical Communication (ECOC), (2017)

[7] M. Arikawa and T. Ito, "Performance of mode diversity reception of a polarization-division-multiplexed signal for free-space optical communication under atmospheric turbulence," Opt. Express 26, 28263-28276 (2018)

[8] Antonin Billaud *et al.*, "Turbulence mitigated single-mode fiber output based on Multi-Plane Light Conversion technology with all-optical coherent recombiner", Proc. SPIE 11852, International Conference on Space Optics — ICSO 2020, 118525X (11 June 2021);

[9] Antonin Billaud *et al.*, "On chip coherent phase and intensity control for atmospheric turbulence mitigation with multi-plane light conversion", Proc. SPIE PC11993, Free-Space Laser Communications XXXIV, PC1199303 (1 April 2022);

[10] V. Billault, J. Bourderionnet, J. P, Mazellier, L. Leviandier, P. Feneyrou, A. Maho, M. Sotom, X. Normandin, H. Lonjaret, and A. Brignon, "Free space optical communication receiver based on a spatial demultiplexer and a photonic integrated coherent combining circuit," Opt. Express 29, 33134-33143 (2021)

[11] Antonin Billaud *et al.*, Mode collection efficiency of atmospheric turbulence mitigation technique based on multiplane light conversion,Proc. SPIE 11532, Environmental Effects on Light Propagation and Adaptive Systems III, 115320B (20 September 2020)

[12] S. Bade et al., "Fabrication and Characterization of a Mode-selective 45-Mode Spatial Multiplexer based on Multi-Plane Light Conversion," 2018 Optical Fiber Communications Conference and Exposition (OFC), 2018, pp. 1-3.

[13] N. Schwartz. "Précompensation des effets de la turbulence par optique adaptative : application aux liaisons optiques en espace libre". Université Nice Sophia Antipolis, 2009

[14] Marie-Thérèse Velluet, Cyril Petit, Louis Le Leuch, Aurélie Montmerle Bonnefois, Jean-Marc Conan, et al.. PICOLO: turbulence simulator for adaptive optics systems assessment in the context of ground-satellite optical links. SPIE Remote Sensing 2020, Sep 2020, Washington (Online Only), United States. pp.1153207, ⟨10.1117/12.2573954⟩.